Letter

Orbital-designed flat-band model and realization of superconductivity in three-dimensional materials

Yueshao Zheng,[1] Leiqiang Li,[2,*] Nannan Luo,[1] Li-Ming Tang,[1] Yexin Feng,[1] Ke-Qiu Chen,[1] Zhenyu Zhang,[3] and Jiang Zeng[1,†]

[1]*Department of Applied Physics, School of Physics and Electronics, Hunan University, Changsha 410082, China*

[2]*Minjiang Collaborative Center for Theoretical Physics, College of Physics and Electronic Information Engineering, Minjiang University, Fuzhou 350108, China*

[3]*International Center for Quantum Design of Functional Materials (ICQD), Hefei National Research Center for Physical Sciences at the Microscale, University of Science and Technology of China, Hefei 230026, China*

(Received 17 September 2023; accepted 25 April 2024; published 10 May 2024)

Electronic materials with a flat-band provide a fertile foundation for exploiting emerging quantum phenomena. Progress has been made in various two-dimensional (2D) systems, especially in a geometric frustrated kagome lattice system and a moire superlattice system for the study of unconventional superconductivity. However, intrinsic superconductivity has not yet been reported in 3D flat-band systems. The orbital degree of freedom might bring new vitality into the field of flat bands and superconductivity. Here, we propose an orbital-designed 3D flat-band model and its realization in various materials containing degenerate p-electrons, d-electrons, or molecular orbitals. More importantly, the possibility of superconductivity in some of these 3D flat-band materials, e.g., K_2Pb and K_2Bi, is revealed via first-principles calculations. Interestingly, these are intrinsically multiband superconductors. Our findings would expand the scope of flat-band studies, shedding light on the exploration of interacting effects and emerging quantum phases in 3D materials.

DOI: 10.1103/PhysRevB.109.L180504

Introduction. The intriguing phenomenon of flat-bands is characterized by a complete absence of dispersion in momentum space due to destructive wave interference. In flat-bands, the kinetic energy is suppressed, making electron-electron interactions dominant. As a result, exploring the interaction effects and unconventional superconductivity in a flat-band system is emerging as a new frontier in fundamental physics [1–9]. In recent years, flat-bands have been experimentally observed in layered materials, such as Fe_3Sn_2 [10], CoSn [11,12], and CsV_3Sb_5 [13,14], possessing frustrated kagome lattices. Moreover, partially filled flat-bands have been experimentally manipulated in the twisted graphene superlattices, exhibiting Mott-insulating phases and unconventional superconductivity [15,16]. Although progress has been made in these two-dimensional (2D) systems, it is still a challenge to realize the high-temperature superconductivity based on an unconventional flat-band, rendering the relationship between the two still mysterious.

Note that the relatively low carrier density in twisted layered systems, and the thermal fluctuations in the 2D limit, would conflict with the realization of long-range ordering at elevated temperature. The 3D system would be a prospective foundation for the study of electronic flat-bands and to further enhance the transition temperature of emerging interaction phases [17]. For example, the 3D pyrochlore lattice stands out as a support for completely flat-bands and the realization of ferromagnetism [18–20] and superconductivity when the flat-band is partially filled via doping [21]. However, intrinsic superconductivity in a 3D flat-band system has not yet been reported, largely due to the lack of proper material realization. The underlying reason is that the realistic 3D flat-band model is relatively rare based on a conventional lattice geometric frustration mechanism [10–28]. In addition to the geometric frustration, the orbital degree of freedom provides a new perspective for the realization of flat-bands [29–32]. By the way, it has been verified that several kagome systems are multiorbital superconductors [14,33,34], and a multi orbital model is necessary to reveal the hidden higher-order topological phase in a MoS_2 monolayer [35]. We proposed that the orbital degree of freedom be conducive to the design and realization of flat-bands beyond the existing geometric frustration models.

In this Letter, we present an orbital-designed 3D flat-band model in the face-centered-cubic (fcc) structure. By considering threefold-degenerate orbitals at the 4a Wyckoff position, we find that the highest energy band is completely flat over the entire 3D Brillouin zone. Employing tight-binding (TB) modeling and first-principles density-functional-theory (DFT) calculations, we uncover that this kind of 3D flat-band can be realized in many materials beyond the existing flat-band database [36]. For examples, it widely exists in conventional alkali-metal chalcogenides K_2X (X = S, Se, or Te) with $p_{x,y,z}$ orbitals, compounds like $Rb(BH)_3$ with degenerate molecular orbitals, and alloy materials including K_2Pb and K_2Bi with degenerate t_{2g} orbitals (d_{xy}, d_{xz}, d_{yz}). Our DFT calculations reveal the possibility of multiband superconductivity in K_2Pb and K_2Bi. Collectively, the central findings presented here extend the realm of 3D flat-band studies and provide insights

*Corresponding author: lilq2022@mju.edu.cn
†jiangzeng@hnu.edu.cn

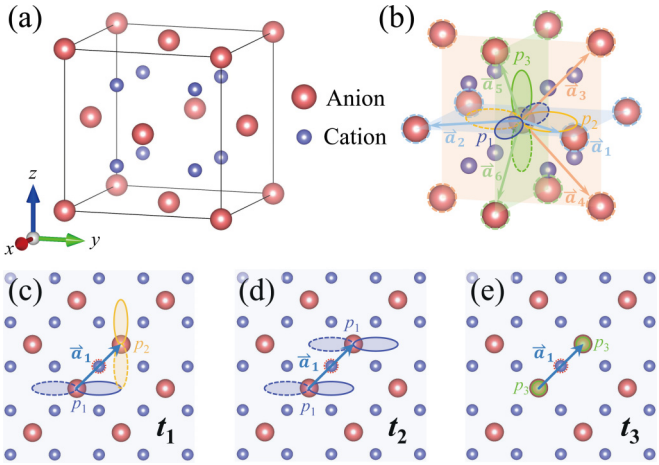

FIG. 1. Tight-binding model of a 3D flat-band based on threefold-degenerate orbitals. (a) Geometrical structure of an fcc lattice, which contains eight tetrahedral sites (cation site) in the unit cell. (b) Schematic diagram of $p_{1,2,3}$-orbitals on the anion represented in blue, gold, and green, respectively (see also the xy, yz, and xz planes). The arrows indicate the lattice vectors in each plane. (c)–(e) Schematic diagrams of the hoppings between p-orbitals along the $\boldsymbol{a}_1$ direction. The red dashed circle donates the nearest cations.

into the exploration of unconventional superconductivity in realistic materials.

Theoretical Model. We start with an orbital-designed three-band TB model. Here, we consider a fcc structure consisting of one site (anion site) per unit cell, as shown in Fig. 1(a). The active electrons live in degenerate p-orbitals of the anion. For convenience, $p_{x,y,z}$ are labeled as $p_{1,2,3}$ and their polarization directions are aligned along the unit vectors of the three orthogonal axes, as shown in Fig. 1(b). For each anion, there are 12 nearest neighbors [see Fig. 1(b) and Fig. S1 of the Supplemental Material] [37]. They lay in three orthogonal planes (xy-, yz-, and xz-plane). In each plane, there are nearest neighbors. Taking into consideration the electron hopping between the nearest neighbors, there are three hopping types in each plane: t_1 describes the hopping between p-orbitals with mutually perpendicular polarization directions; t_2 and t_3 donate the hopping between the same p-orbitals, where the p-orbitals in the t_3 hopping type are perpendicular to the hopping direction. For more details of the structure and TB modeling, see the Supplemental Material [37].

The values of t_1 and t_2 are approximately equal since they share an identical projection from the σ- and π-bonding terms. The relative value of t_1 and t_3 depends on materials and can be tuned by external pressure. A completely flat-band appears in the case of $t_1 = t_2 = t_3 = t$. The flat-band Hamiltonian of the TB model can be written in a symmetric format,

$$H = \sum_k \Psi_k^\dagger h_k \Psi. \tag{1}$$

The basis is $\Psi_k^\dagger = (p_{1,k}^\dagger,\ p_{2,k}^\dagger,\ p_{3,k}^\dagger)$ and h_k expressed as

$$-4t \begin{pmatrix} \Lambda_1 & -\sin k_x \sin k_y & -\sin k_z \sin k_x \\ -\sin k_x \sin k_y & \Lambda_2 & -\sin k_y \sin k_z \\ -\sin k_z \sin k_x & -\sin k_y \sin k_z & \Lambda_3 \end{pmatrix}, \tag{2}$$

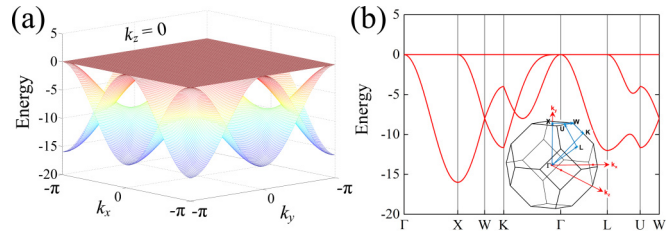

FIG. 2. Energy dispersion of the 3D multiorbital TB model. (a) 3D band structure for h_k with the parameters $t_1 = t_2 = t_3 = -1$ and $k_z = 0$. (b) 2D band structure along the high-symmetry directions. The inset is the Brillouin zone and high-symmetry path.

where

$$\Lambda_1 = \cos k_x \cos k_y + \cos k_z \cos k_x - \cos k_y \cos k_z, \tag{3}$$

$$\Lambda_2 = \cos k_x \cos k_y + \cos k_y \cos k_z - \cos k_z \cos k_x, \tag{4}$$

$$\Lambda_3 = \cos k_y \cos k_z + \cos k_z \cos k_x - \cos k_x \cos k_y. \tag{5}$$

To explicitly show the flat-band, we plot the 3D band structure of h_k at $k_z = 0$ in Fig. 2(a). There are two dispersive bands $E_k^{(1)} = -4t(\cos k_x + \cos k_y - \cos k_x \cos k_y)$ and $E_k^{(2)} = -4t(2\cos k_x \cos k_y - 1)$, and one flat-band $E_k^{(3)} = -4t$. The dispersive bands and flat-band touch at the center of the Brillouin zone. The bands $E^{(1)}$ and $E^{(3)}$ are energetically degenerate along the $k_x = 0$ and $k_y = 0$ lines. The wave function of the flat-band is mainly localized at the anion sites. It is emphasized that $E_k^{(3)} = -4t$ remains dispersionless at arbitrary k points and is totally flat over the entire 3D Brillouin zone, as shown in Fig. 2(b). The totally flat-band is attributed to the frustrated hopping nature. The loop in Fig. S2 represents a compact localized state and the frustrated hopping to a neighbor orbital.

Materials Realization. The above 3D flat-band would be widespread in materials with fcc structures. Via first-principles calculations, we proposed several classes of materials for its realization. Alkali-metal chalcogenides I_2VI within antifluorite-type structure, made from elements in the I and VI main group, were already synthesized over nine decades ago [38] and widely used in analytical reagents [39], the pharmaceutical industry [40], and solid-state batteries [41]. In antifluorite-type structure, the anions form an fcc lattice and the cations form a simple cubic lattice. Here, we take K_2Te as an example. The optimized lattice constant of K_2Te is about 5.82 Å. Figure 3(a) shows the electronic band structure and atomic orbital projected density of states (DOS) of K_2Te. The three electronic bands at the valence edge mainly come from the p-orbitals of a Te atom. The top bands are nearly flat in the whole Brillouin zone with a narrow bandwidth of 57 meV, as shown in Fig. 3(a), which is well-fitted by our TB model. The predicted $Na_6S_2O_9$ exhibit more complex structures relative to alkali-metal chalcogenides (see Fig. S4). In $Na_6S_2O_9$, there are two types of O atoms, namely O(I) and O(II). The O(I) atom is located at the 4a site and bonded in an octahedral geometry to six Na atoms, while four O(II) atoms and one S atom form a tetrahedral geometry. Three valence bands almost come from the p-orbitals of an O(I) atom, where the topmost band is a completely flat-band with a bandwidth of 22 meV.

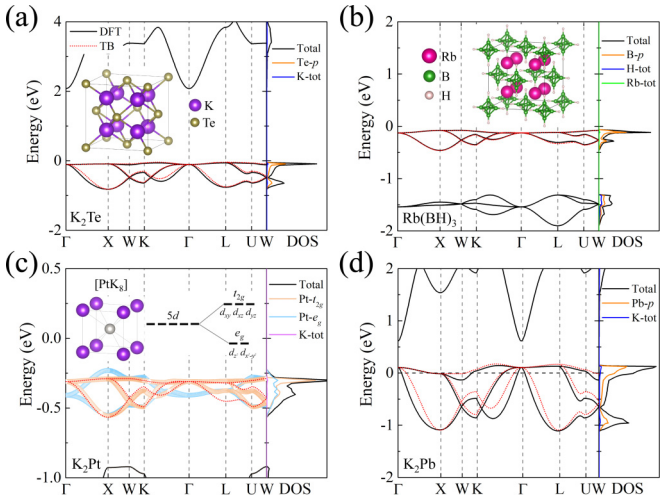

FIG. 3. Atomic and electronic structure for fcc crystals of (a) K_2Te, (b) $Rb(BH)_3$, (c) K_2Pt, and (d) K_2Pb. Black solid curves and red filled dots represent the DFT results and TB fittings, respectively.

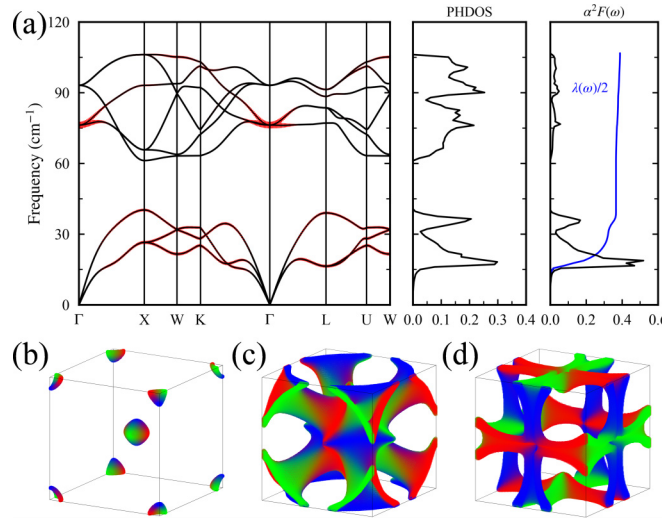

FIG. 4. Phonon dispersion and Fermi surfaces of K_2Pb. (a) Phonon dispersion and phonon linewidth (represented by red circles) along a standard high-symmetry path, phonon DOS, Eliashberg spectral function $\alpha^2F(\omega)$, and frequency-dependent electron-phonon coupling constant $\lambda(\omega)$ for K_2Pb. (b)–(d) Distributions of p-orbitals on the Fermi surfaces. Red, green, and blue represent the p_x, p_y, and p_z orbitals, respectively.

Molecular orbitals can also form a similar 3D flat-band structure. For $Rb(BH)_3$, Rb atoms occupy the 8c (0.25, 0.25, 0.25) Wyckoff position, while B and H atoms sit at (0.5, 0.5, 0.87) and (0.5, 0.5, 0.74) positions, respectively. Each H atom is bonded to a B atom, and every six B atoms form an octahedron, as shown in the inset of Fig. 3(b). Here, we can consider the B octahedron and the H atoms bonded to it as a molecule "B," so that the chemical formula $Rb(BH)_3$ can be transformed into the Rb_2 "B," like the alkali-metal chalcogenides mentioned above. Figure 3(b) shows the band structure of $Rb(BH)_3$. Electronic bands near the Fermi level come from the p-orbitals of B atoms. The topmost valence band is a flat-band with a bandwidth of 49 meV. This flat-band will become more dispersive when Rb atoms are replaced by K or Cs atoms (see Fig. S5).

The TB model is also suitable for d-orbitals materials. In an fcc structure, the metal atom M forms $[MX_8]$ with eight surrounding X atoms, leading to the splitting of the d-orbitals into t_{2g} and e_g subsets. The degenerate t_{2g} orbitals (d_{xy}, d_{xz}, d_{yz}) in an fcc lattice contribute an electronic flat-band similar to the cases of degenerate p-orbitals. For example, K_2Pt metal–alkali-metal alloy is fluorite-structured and crystallizes in the cubic $Fm\bar{3}m$ space group. Figure 3(c) shows the orbital-projected band structures. It is clear that the five d-orbital bands are divided into two groups separated by a crystal-field-splitting energy. The top band from t_{2g} orbitals is completely flat, with a bandwidth of 38 meV. For K_3Ir at the pressure of 15 GPa, the flat-band consisting of t_{2g} orbitals moves away from the e_g orbitals due to the larger crystal-field-splitting energy relative to K_2Pt (see Fig. S6). The K_3Ir could also be stabilized in $Fm\bar{3}m$ structure at a pressure of 15 GPa with an energy of 37 meV per atom higher than that of the $Pmnm$ phase [42]. In addition, in the ferromagnetic semimetals $C_{14}Cl_{12}H_{24}MnN_8Nb_6$ and $BBr_{20}K_8Zr_6$, the d-orbitals of Nb and Zr atoms form flat-bands (Figs. S7 and S8), respectively. For Ca_2FeH_6 and Sr_2FeH_6, which contain $[FeH_6]$ octahedra, we also show similar flat-band structures (Fig. S9). Phonon calculations determine their dynamical stability (Fig. S10).

Superconductivity. Finally, we turn our attention to superconducting properties. It is well known that the superconducting critical temperature T_c depends exponentially on the electronic density of states and the attractive electron-electron interaction in conventional superconductors. In flat-band systems, the divergent density of states would give rise to a parametrically enhanced T_c that is linear in the strength of interaction, indicating the possibility of a robust superconducting phase. Interest in flat-band superconductivity has surged in recent years with the experimental observation of twisted graphene superlattices [43–49]. Although unconventional superconductivity has been verified in some of these systems, their T_c's are relatively low. We propose here that the T_c might be enhanced in a 3D flat-band system since thermal fluctuations, which are destructive in 2D systems, would not dominate in 3D cases. In the framework of Bardeen-Cooper-Schrieffer (BCS) theory, we investigate the possibility of superconductivity in K_2Pb, whose flat-bands are partially filled, as shown in Fig. 3(d). Note that for 3D flat-band systems, the T_c achieved here from the BCS theory is just a verification of superconductivity rather than an accurate result.

Figure 4(a) shows the phonon-dispersion relations and the electron-phonon linewidths of K_2Pb, together with the phonon DOS and the Eliashberg spectral functions. The stability of K_2Pb is ascertained by the nonimaginary phonon spectra. It has a small frequency gap at around 45 cm^{-1}, with a gap value of about 2.4 meV. The optical-phonon modes with frequencies of 75 cm^{-1} possess strong coupling with electrons. By integrating $\alpha^2F(\omega)$, the electron-phonon coupling (EPC) constant λ is equal to 0.78. Using the McMillan-Allen-Dynes formula and setting the screened Coulomb potential μ^* to 0.1 (0.16),

the T_c of K_2Pb is estimated to be 1.42 (0.88) K. By replacing Pb with Bi, the T_c is enhanced to about 2.2 K ($\mu^* = 0.1$) [Fig. S11(a)]. The critical temperature T_c of superconductivity will be affected by the DOS at the Fermi level. The pressure can basically shift the position of the flat-band relative to the Fermi level, thereby altering the DOS and then T_c. Under external pressure, the T_c in K_2Os (5 GPa) and K_2Ir (5 GPa) is about 0.2 and 1.3 K [see Figs. S11(b) and 11(c)], respectively. The superconducting critical temperature will be affected due to the significant impact of the large spin-orbit coupling effects on the flat-band structure, as shown in Figs. S12 and S13 of the Supplemental Material. It is noteworthy that the $p_{x,y,z}$-orbitals on the Fermi surfaces are evenly distributed, confirming multiorbital (multiband) superconductivity here. Although the superconducting transition temperatures are not high in the framework of BCS theory, this may provide a viable route to high-temperature flat-band superconductivity, which is currently a subject of tremendous interest.

Discussion. Unconventional superconductivity associated with flat-bands has recently been uncovered in various 2D systems, including twisted graphene superlattices and layered kagome metals [14,50,51]. However, the critical temperature T_c is relatively low in the range of 0.9–2.5 K. In the 2D limit, the long-range ordering would inevitably be suppressed by thermal fluctuations. This would result in the challenge of a further increase in the superconducting T_c despite the presence of flat-bands. In addition, some layered kagome metals are experimentally revealed as multiband superconductors in which van Hove singularities at the Fermi level play a predominant role, indicating that a single-orbital flat-band might not directly engage in superconductivity [52,53]. It would be worthwhile to continue to explore how a flat-band can be used to enhance superconductivity. The 3D materials with partially filled flat-bands would provide a strong foundation for the exploration of unconventional superconductivity. Although the T_c of unconventional superconductivity might not be accurately estimated in the BCS framework, the desired superconductivity directly driven by a 3D flat-band was somehow verified in the alloys, such as K_2Bi, K_2Pb, K_2Os, and K_2Ir. In addition, these 3D flat-band materials are beyond the reported flat-band database [36].

Conclusions. We have proposed an orbital-designed 3D flat-band model and its material realization of superconductivity. In this theoretical model, the electronic band exhibits complete flatness throughout the 3D Brillouin zone due to the destructive interference between the degenerate orbitals rather than the conventional lattice geometric frustration. Taking advantage of the prevalence of degenerate valence electrons in elements and the common fcc structure, the proposed flat-band exists in several classes of materials with degenerate $p_{x,y,z}$-orbitals, t_{2g}-type d-orbitals, or effectively molecular orbitals around the electron Fermi level. In some alloys, the flat-band is partially filled by the d-electrons. BCS theory is adapted to estimate the interaction strength and the possibility of superconductivity in K_2Bi, K_2Pb, K_2Os, and K_2Ir as concrete examples. These findings not only extend the realm of 3D flat-band studies, but they also offer promising opportunities for the experimental observation of flat-bands and superconductivity in realistic materials.

Note added. After the submission of this Letter, a report appeared on the experimental realization of a 3D flat-band and its superconductivity via heavy doping [21], while the realization of intrinsic superconductivity in 3D flat-band material remains a challenge.

Acknowledgments. The authors thank Wei Qin at the University of Science and Technology of China, and Feng Liu at the University of Utah for helpful discussions. This work was supported by the National Key Research and Development Program of Ministry of Science and Technology (Grant No. 2022YFA1402504) and the National Natural Science Foundation of China (Grants No. 62201208, No. 12074112, and No. 11974105). The Natural Science Foundation of Fujian Province of China (Grant No. 2023J05248) and the start-up fund of Minjiang University (Grant No. 30804327).

[1] S. D. Huber and E. Altman, Phys. Rev. B **82**, 184502 (2010).
[2] A. Julku, G. M. Bruun, and P. Törmä, Phys. Rev. Lett. **127**, 170404 (2021).
[3] H. Tasaki, Prog. Theor. Phys. **99**, 489 (1998).
[4] H. Tasaki, Phys. Rev. Lett. **69**, 1608 (1992).
[5] S. Zhang, H. H. Hung, and C. Wu, Phys. Rev. A **82**, 053618 (2010).
[6] J.-X. Yin, S. S. Zhang, G. Chang, Q. Wang, S. S. Tsirkin, Z. Guguchia, B. Lian, H. Zhou, K. Jiang, I. Belopolski *et al.*, Nat. Phys. **15**, 443 (2019).
[7] Y.-F. Wang, Z.-C. Gu, C.-D. Gong, and D. N. Sheng, Phys. Rev. Lett. **107**, 146803 (2011).
[8] E. Tang, J.-W. Mei, and X.-G. Wen, Phys. Rev. Lett. **106**, 236802 (2011).
[9] K. Kobayashi, M. Okumura, S. Yamada, M. Machida, and H. Aoki, Phys. Rev. B **94**, 214501 (2016).
[10] Z. Lin, J.-H. Choi, Q. Zhang, W. Qin, S. Yi, P. Wang, L. Li, Y. Wang, H. Zhang, Z. Sun *et al.*, Phys. Rev. Lett. **121**, 096401 (2018).
[11] M. Kang, S. Fang, L. Ye, H. C. Po, J. Denlinger, C. Jozwiak, A. Bostwick, E. Rotenberg, E. Kaxiras, J. G. Checkelsky *et al.*, Nat. Commun. **11**, 4004 (2020).
[12] H. Huang, L. Zheng, Z. Lin, X. Guo, S. Wang, S. Zhang, C. Zhang, Z. Sun, Z. F. Wang, H. Weng, L. Li, T. Wu, X. Chen, and C. Zeng, Phys. Rev. Lett. **128**, 096601 (2022).
[13] Y. Hu, S. M. Teicher, B. R. Ortiz, Y. Luo, S. Peng, L. Huai, J. Ma, N. C. Plumb, S. D. Wilson, J. He *et al.*, Sci. Bull. **67**, 495 (2022).
[14] R. Lou, A. Fedorov, Q. Yin, A. Kuibarov, Z. Tu, C. Gong, E. F. Schwier, B. Büchner, H. Lei, and S. Borisenko, Phys. Rev. Lett. **128**, 036402 (2022).
[15] Y. Cao, V. Fatemi, A. Demir, S. Fang, S. L. Tomarken, J. Y. Luo, J. D. Sanchez-Yamagishi, K. Watanabe, T. Taniguchi, E. Kaxiras *et al.*, Nature (London) **556**, 80 (2018).
[16] J. M. Park, Y. Cao, L.-Q. Xia, S. Sun, K. Watanabe, T. Taniguchi, and P. Jarillo-Herrero, Nat. Mater. **21**, 877 (2022).
[17] A. Drozdov, M. Eremets, I. Troyan, V. Ksenofontov, and S. I. Shylin, Nature (London) **525**, 73 (2015).

[18] Y. Zhou, K.-H. Jin, H. Huang, Z. Wang, and F. Liu, Phys. Rev. B **99**, 201105(R) (2019).
[19] I. Hase, T. Yanagisawa, Y. Aiura, and K. Kawashima, Phys. Rev. Lett. **120**, 196401 (2018).
[20] H.-M. Guo and M. Franz, Phys. Rev. Lett. **103**, 206805 (2009).
[21] J. P. Wakefield, M. Kang, P. M. Neves, D. Oh, S. Fang, R. McTigue, S. Frank Zhao, T. N. Lamichhane, A. Chen, S. Lee *et al.*, Nature (London) **623**, 301 (2023).
[22] A. Mielke, J. Phys. A **24**, 3311 (1991).
[23] A. Mielke, J. Phys. A **24**, L73 (1991).
[24] S. Miyahara, K. Kubo, H. Ono, Y. Shimomura, and N. Furukawa, J. Phys. Soc. Jpn. **74**, 1918 (2005).
[25] C. S. Chiu, D.-S. Ma, Z.-D. Song, B. A. Bernevig, and A. A. Houck, Phys. Rev. Res. **2**, 043414 (2020).
[26] T. Misumi and H. Aoki, Phys. Rev. B **96**, 155137 (2017).
[27] W. Maimaiti, A. Andreanov, H. C. Park, O. Gendelman, and S. Flach, Phys. Rev. B **95**, 115135 (2017).
[28] A. Graf and F. Piéchon, Phys. Rev. B **104**, 195128 (2021).
[29] H. Liu, G. Sethi, S. Meng, and F. Liu, Phys. Rev. B **105**, 085128 (2022).
[30] Z. Liu, Z. F. Wang, J.-W. Mei, Y.-S. Wu, and F. Liu, Phys. Rev. Lett. **110**, 106804 (2013).
[31] C. Wu, D. Bergman, L. Balents, and S. Das Sarma, Phys. Rev. Lett. **99**, 070401 (2007).
[32] J. Zeng, M. Lu, H. Liu, H. Jiang, and X. C. Xie, Sci. Bull. **66**, 765 (2021).
[33] T. Neupert, M. M. Denner, J.-X. Yin, R. Thomale, and M. Z. Hasan, Nat. Phys. **18**, 137 (2022).
[34] C. Mielke III, Y. Qin, J.-X. Yin, H. Nakamura, D. Das, K. Guo, R. Khasanov, J. Chang, Z. Q. Wang, S. Jia, S. Nakatsuji, A. Amato, H. Luetkens, G. Xu, M. Z. Hasan, and Z. Guguchia, Phys. Rev. Mater. **5**, 034803 (2021).
[35] J. Zeng, H. Liu, H. Jiang, Q.-F. Sun, and X. C. Xie, Phys. Rev. B **104**, L161108 (2021).
[36] N. Regnault, Y. Xu, M.-R. Li, D.-S. Ma, M. Jovanovic, A. Yazdani, S. S. Parkin, C. Felser, L. M. Schoop, N. P. Ong *et al.*, Nature (London) **603**, 824 (2022).
[37] See Supplemental Material at http://link.aps.org/supplemental/10.1103/PhysRevB.109.L180504 for the details of the orbital-designed TB model, electronic structures, and TB fittings of all predicted fcc crystals, and the lattice dynamics of alloy materials.
[38] E. Zintl, A. Harder, and B. Dauth, Z. Elektrochem. Angew. Phys. Chem. **40**, 588 (1934).
[39] S. Licht, F. Forouzan, and K. Longo, Anal. Chem. **62**, 1356 (1990).
[40] P. Maity and B. C. Ranu, Adv. Synth. Catal. **359**, 4369 (2017).
[41] J. Jiang, Y. Liu, Y. Liao, W. Li, Y. Xu, X. Liu, Y. Jiang, J. Zhang, and B. Zhao, Small **19**, 2300854 (2023).
[42] J. Brgoch and M. Hermus, J. Phys. Chem. C **120**, 20033 (2016).
[43] F. Wu and S. Das Sarma, Phys. Rev. B **101**, 155149 (2020).
[44] J. Y. Lee, E. Khalaf, S. Liu, X. Liu, Z. Hao, P. Kim, and A. Vishwanath, Nat. Commun. **10**, 5333 (2019).
[45] H. Kim, Y. Choi, C. Lewandowski, A. Thomson, Y. Zhang, R. Polski, K. Watanabe, T. Taniguchi, J. Alicea, and S. Nadj-Perge, Nature (London) **606**, 494 (2022).
[46] J. M. Park, Y. Cao, K. Watanabe, T. Taniguchi, and P. Jarillo-Herrero, Nature (London) **590**, 249 (2021).
[47] Z. Hao, A. Zimmerman, P. Ledwith, E. Khalaf, D. H. Najafabadi, K. Watanabe, T. Taniguchi, A. Vishwanath, and P. Kim, Science **371**, 1133 (2021).
[48] L. Balents, C. R. Dean, D. K. Efetov, and A. F. Young, Nat. Phys. **16**, 725 (2020).
[49] G. Chen, A. L. Sharpe, P. Gallagher, I. T. Rosen, E. J. Fox, L. Jiang, B. Lyu, H. Li, K. Watanabe, T. Taniguchi *et al.*, Nature (London) **572**, 215 (2019).
[50] B. R. Ortiz, P. M. Sarte, E. M. Kenney, M. J. Graf, S. M. L. Teicher, R. Seshadri, and S. D. Wilson, Phys. Rev. Mater. **5**, 034801 (2021).
[51] Q. Yin, Z. Tu, C. Gong, Y. Fu, S. Yan, and H. Lei, Chin. Phys. Lett. **38**, 037403 (2021).
[52] S. Cho, H. Ma, W. Xia, Y. Yang, Z. Liu, Z. Huang, Z. Jiang, X. Lu, J. Liu, Z. Liu *et al.*, Phys. Rev. Lett. **127**, 236401 (2021).
[53] Y. Hu, X. Wu, B. R. Ortiz, S. Ju, X. Han, J. Ma, N. C. Plumb, M. Radovic, R. Thomale, S. D. Wilson *et al.*, Nat. Commun. **13**, 2220 (2022).